

Alternative approach to all-angle-negative-refraction in two-dimensional photonic crystals

Y. J. Huang, W. T. Lu,* and S. Sridhar†

Department of Physics and Electronic Materials Research Institute,
Northeastern University, Boston, Massachusetts 02115, USA

(Dated: September 26, 2018)

We show that with an appropriate surface modification, a slab of photonic crystal can be made to allow wave transmission within the photonic band gap. Furthermore, negative refraction and all-angle-negative-refraction (AANR) can be achieved by this surface modification in frequency windows that were not realized before in two-dimensional photonic crystals [C. Luo et al, Phys. Rev. B **65**, 201104 (2002)]. This approach to AANR leads to new applications in flat lens imaging. Previous flat lens using photonic crystals requires object-image distance $u + v$ less than or equal to the lens thickness d , $u + v \sim d$. Our approach can be used to design flat lens with $u + v = \sigma d$ with $\sigma \gg 1$, thus being able to image large and/or far away objects. Our results are confirmed by FDTD simulations.

PACS numbers:

I. INTRODUCTION

Negative refraction (NR) was proposed theoretically a long time ago [1]. It was realized only recently in two classes of materials. One type is the so-called metamaterials [2–4], consisting of wires and split-ring resonators. The second type is photonic crystals [5], which have periodic permittivity and/or permeability.

In these artificial materials, there are up to now two mechanisms to achieve negative refraction (NR). One is to use the anti-parallelism between the wave vector and the group velocity [6]. This can be realized in isotropic metamaterials [2] and in the second or even higher band around the Γ point in photonic crystals (PCs) [6]. In this case, the phase refractive index n_p is negative.

The second mechanism is to use the anisotropy and the concavity of the equi-frequency surface (EFS) such as the EFS around the M point in the first band of a square lattice PC. In this case though the phase refractive index n_p is positive, the group refractive index n_g is negative [7]. In order to show negative lateral shift or all-angle-negative-refraction (AANR), one has to orient the lattice such that the ΓM direction is along the surface normal. Negative refraction and flat lens imaging [8] using both mechanisms have been observed in microwave [9–15] and near infrared experiments [16].

Recently we proposed a new mechanism for negative refraction using surface grating [17]. This mechanism combines photonic band gap with surface grating to achieve NR and AANR. Negative lateral shift and AANR have been demonstrated in a multilayered structure with surface grating.

In this paper, we obtain new windows of AANR in two-dimensional (2D) PCs using this new mechanism of surface modification. We also show that flat lens made of

photonic crystal with surface grating can have $u + v = \sigma d$ [18] with $\sigma \gg 1$ while for the Veselago-Pendry flat lens [8] $\sigma = 1$. Here d is the thickness of the flat lens, u and v are the distance from the lens to the object and the image, respectively. Thus a flat lens can focus large and far away objects.

II. NEW APPROACH TO AANR

In a pioneering paper [7], Luo et al showed that within certain frequency windows in the first band of a PC, AANR can be achieved. Specifically, within the first band, AANR is possible only along the ΓM direction for a square lattice PC. We will show that with appropriate surface grating, NR and AANR is possible along the ΓX direction in the first band of a square lattice PC.

In the main text of this paper, we only consider the transverse magnetic (TM) modes of a square lattice PC of square rods. Square lattice of circular rods or even rhombus rods can be treated similarly. The generalization to transverse electric (TE) modes and lattice structures other than square lattice is straightforward. As a specific example, we consider a square lattice of square rods with size $b/a = 0.7$, thus a filling ratio of 0.49. The EFS is of this PC is calculated using the plane-wave expansion [5] with 5041 plane waves. The EFS of the first band is shown in Fig. 1. The frequencies at the X point and the M point are $\omega_X = 0.1943 \times 2\pi c/a$ and $\omega_M = 0.2446 \times 2\pi c/a$, respectively.

Consider a slab of this PC with surface normal along the ΓX direction. If one increases the frequency, $\omega > \omega_X$, there will be a partial band gap for waves incident to the air-PC interface since the Bloch waves have $k_y \geq k_a$ and the incident plane wave with $k_y < k_a$ will be completely reflected. Here k_a is the k_y value of the crossing point of the EFS with the XM boundary of the first Brillouin zone, as can be seen in Fig. 1 and Fig. 2. For certain frequencies $\omega_l < \omega < \omega_M$ with $\omega_l = 0.2089 \times 2\pi c/a$ when $k_a = \omega/c$, a flat slab of such PC is an omnidirectional

*Electronic address: w.lu@neu.edu

†Electronic address: s.sridhar@neu.edu

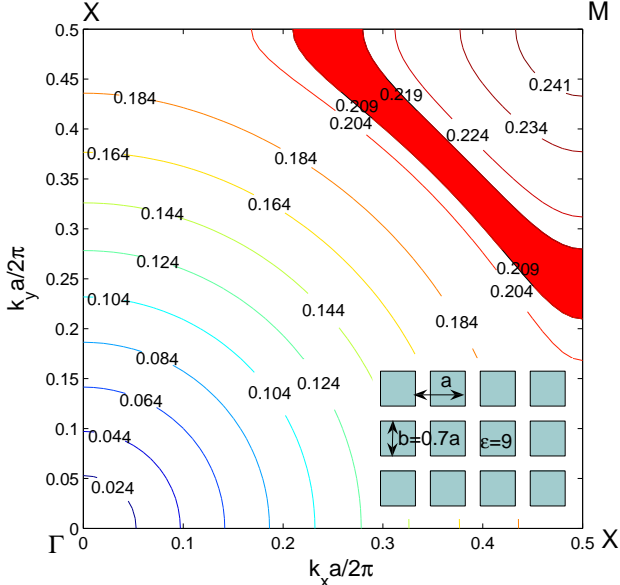


FIG. 1: (Color online) EFS of the TM modes of a square lattice PC. The lattice is made of square rods of alumina ($\epsilon = 9$) with filling ratio 0.49 (see insert). The shading area is the window of AANR for the PC with surface grating $a_s = 2a$ (see Fig. 3). A slab of this PC is oriented such that the surface normal is along the ΓX direction.

reflector [19]. For example for $\omega = 0.219 \times 2\pi c/a$ as shown in Fig. 2, there will be total external reflection for any incident plane wave. However for these frequencies, a surface grating with period

$$a_s = 2a \quad (1)$$

will give a momentum boost along the surface to the incident plane wave with incident angle θ such that it will be coupled to the Bloch waves inside the PC with transverse momentum $k_y = \pi/a + (\omega/c) \sin \theta$ if θ is negative and $k_y = -\pi/a + (\omega/c) \sin \theta$ if θ is positive. The refracted wave will propagate on the opposite side of the surface normal with respect to the incident beam. Thus NR is achieved. This is illustrated in Fig. 2. The effect of this surface grating is equivalent to bringing down the EFS around the M point to the X point for $\omega_l < \omega < \omega_M$. As we pointed out in Ref. [17], it is the surface periodicity which determines the size of the EFS and the folding of the band structure. Furthermore, if $\pi/a - k_a \geq \omega/c$, AANR can be achieved. The upper limit for AANR is $\omega_u = 0.2192 \times 2\pi c/a$. Thus we obtained a 4.7% AANR around ω_u .

The above approach to NR and AANR is confirmed in our numeric simulations using FDTD [20]. Here we consider the lateral shift of an incident beam by a slab made of a square lattice PC. The detail of the slab is shown in Fig. 3. Negative lateral shifts are observed for different incident angles as shown in Fig. 4 for beams at $\omega = 0.219 \times 2\pi c/a$. It can be verified that for this slab, AANR can be achieved for $0.2089 \leq \omega a/2\pi c \leq 0.2192$. Note that the details of the surface grating is not

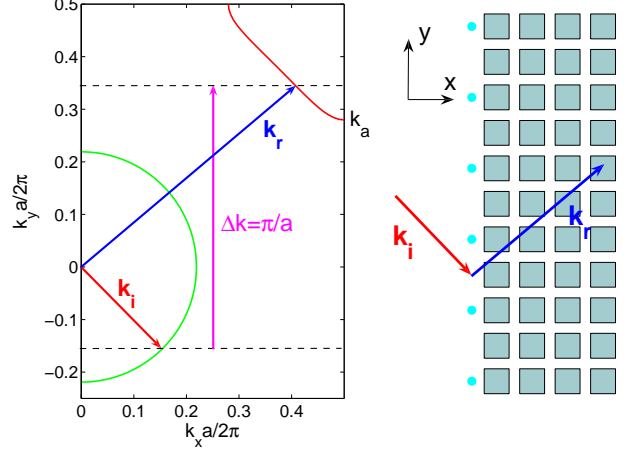


FIG. 2: (Color online) Mechanism for NR and AANR for a square lattice PC with surface grating $a_s = 2a$. The red curve is the EFS in the PC and the green one is that in the air for $\omega = 0.219 \times 2\pi c/a$. With the momentum kick $\Delta k = \pi/a$, an incident plane wave with \vec{k}_i will be refracted negatively into a plane wave with \vec{k}_r .

essential except its period $a_s = 2a$. The grating can be holographic or an array of circular rods as long as it is not too thick. For the specific surface grating shown in Fig. 3, the energy transmissions are 99.2% and 4.7% for plane waves with incident angles 15° and 30°, respectively.

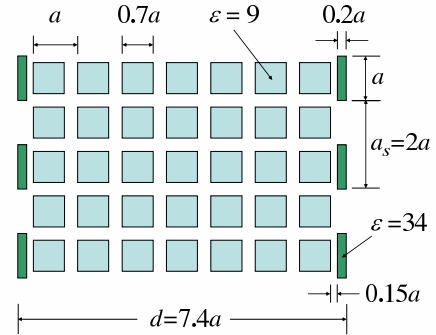


FIG. 3: (Color online) Details of slab made of a square lattice PC with surface grating $a_s = 2a$. For simplicity, the thickness d of the slab is defined as the distance from the first surface to the last surface of the structure.

III. FLAT LENS WITH LARGE σ

One prominent application of negative refraction is the Veselago-Pendry perfect lens [8]. A flat slab of thickness d can focus an object with distance u on one side to a distance v on the other side with $u+v = d$ if the refractive index $n = -1$. For a generalized flat lens without optical axis [18], the lens equation takes the form

$$u+v = \sigma d \quad (2)$$

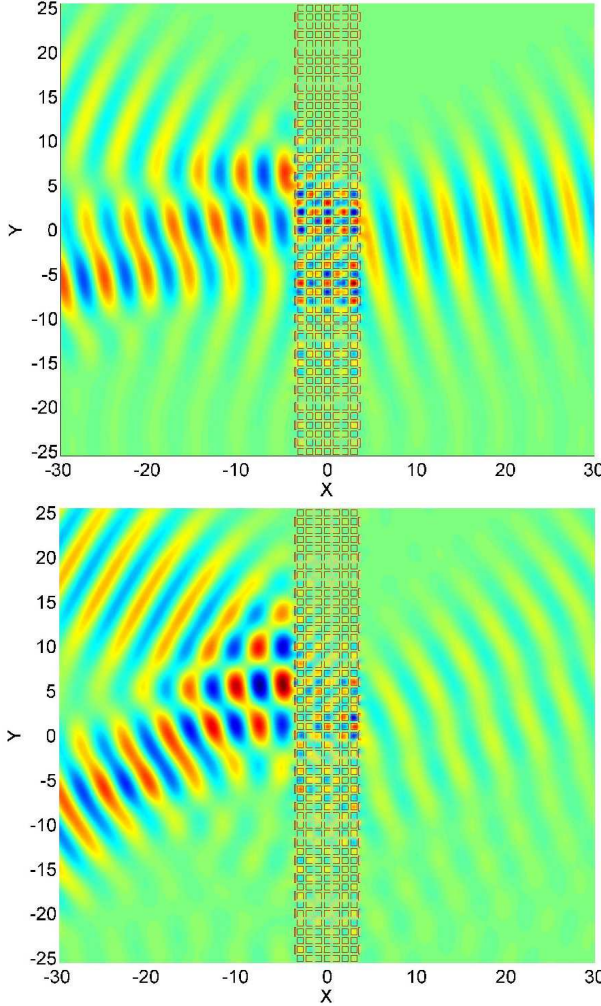


FIG. 4: (Color online) Negative lateral shift by a slab of PC given in Fig. 3 for incident Gaussian beam with incident angles 15° (top) and 30° (bottom) at $\omega = 0.219 \times 2\pi c/a$. The distance is measured in the unit of lattice spacing a .

with σ a material property, depending on the dispersion characteristics of the flat lens. This is illustrated in Fig. 5. This lens equation requires the following form of the EFS at the operating frequency

$$k_{rx} = \kappa - \sigma \sqrt{\omega^2/c^2 - k_y^2}. \quad (3)$$

The lens surface is in the y -direction. The surface normal is along the x -axis. Here k_{rx} is the longitudinal component of the wave vector in the lens medium and κ is the center of the EFS ellipse [18].

Even though AANR can be realized in the first band along the ΓM direction for a square lattice PC [7], the EFS is very flat around the lens normal. Thus one has $\sigma \ll 1$ [18]. Though $\sigma \sim 1$ has been reported in PCs with other structures [21, 22], the focusing is still limited to the vicinity of the lens surface [23]. For practical applications, we need large σ so that the object and image can be far away from the lens. We will show that with our new mechanism for AANR, large σ can be achieved.

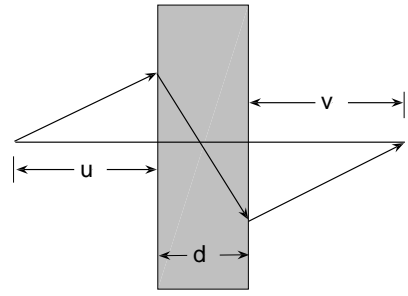


FIG. 5: A flat lens with lens equation $u + v = \sigma d$.

As we have stated in the previous section, the first Brillouin zone of a square lattice PC with surface grating $a_s = 2a$ takes the shape of a rectangle instead of a square and its vertical size is reduced to $-\pi/a \leq k_y \leq \pi/a$. The center of the EFS for $\omega_l \leq \omega \leq \omega_M$ of the original PC is moved from the M point to the X point. The fitting of the modified EFS for these frequency by Eq. (3) will give the lens property σ . An inspection of the band structure reveals that the EFS is not elliptical. This results in incident angle dependent σ [18]. Nevertheless, the EFS can be fitted well with a constant σ_0 for small k_y as shown in Fig. 6. For the square lattice PC we have designed (Fig. 3), one has $\sigma_0 \sim 4$ for $\omega_l \leq \omega \leq \omega_u$.

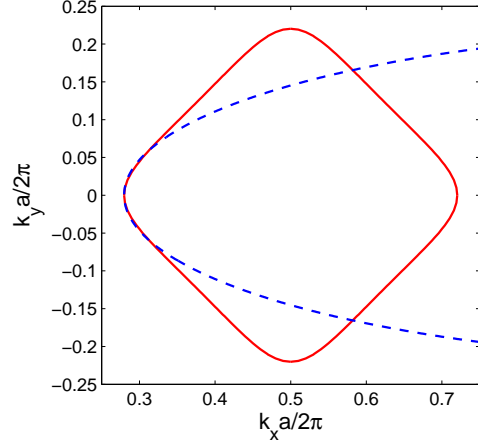


FIG. 6: (Color online) Fitting of EFS of the TM modes at $\omega a/2\pi c = 0.219$ by Eq. (3). Here $\sigma_0 = 4$ and $\kappa a/2\pi c = 1.16$. Note that the center of EFS is shifted from the M point to the X point due to the surface grating $a_s = 2a$.

Focusing by such a flat lens is shown in Fig. 7. For a point source with $u = 13.6a$, a clear focused image is obtained at $v = 12.4a$ for the operating frequency $\omega = 0.219 \times 2\pi c/a$, which is consistent with the lens equation $u + v = \sigma_{\text{eff}} d$ with $\sigma_{\text{eff}} = 3.5$ and $d = 7.4a$. There are two reasons for $\sigma_{\text{eff}} < \sigma_0$. First that the EFS is elliptical only for small $k_y = (\omega/c) \sin \theta$ and $\sigma \equiv -dk_{rx}/dk_x$ decreases with increasing incident angle θ . The effective σ_{eff} is an average and thus smaller than σ_0 . Second, the thickness

of a PC slab is not a well-defined quantity. Here we simply define the lens thickness as the distance from the first surface to the last surface as shown in Fig. 3. This may overestimate the effective thickness of the lens.

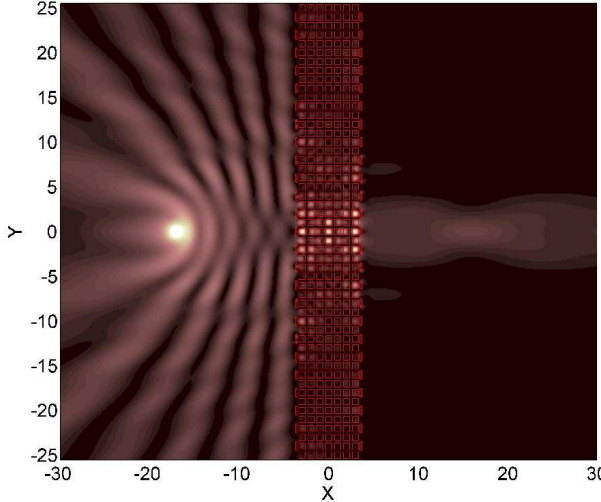


FIG. 7: (Color online) FDTD simulation of flat lens focusing of a point source. For better contrast effect, the field intensity at the point source is suppressed. The detail of the lens is given in Fig. 3.

To further check the performance of this flat lens, we vary the object distance. In Fig. 8 we show that the ratio $(u + v)/d$ is almost constant and very close to σ_0 for different object distance u .

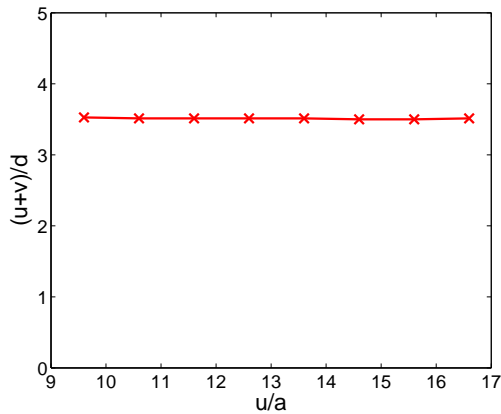


FIG. 8: The ratio of the object-image distance to the slab thickness $(u + v)/d$ vs. the object distance u for the flat lens shown in Fig. 3 at the operating frequency $\omega = 0.219 \times 2\pi c/a$.

The primary concern of practical application is the power transmission through the lens. As expected, the transmission through the flat lens is low due to the impedance mismatch. However since the details of the grating on the PC will not alter the scenario for NR, the power transmission can be enhanced through careful engineering of the grating. In our simulation, we find that the grating on the 2D PC with large dielectric constant

has strong power transmission. The parameters of the surface grating shown in Fig. 3 are not optimized. Further improvement of transmission may be possible. For the grating parameters given in Fig. 3, the transmission coefficient is calculated and plotted in Fig. 9.

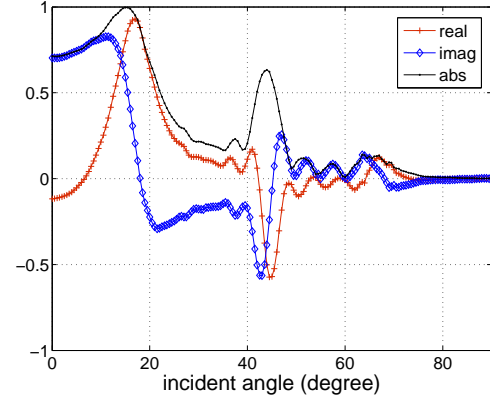


FIG. 9: (Color online) The transmission coefficient for plane wave incident on the flat lens shown in Fig. 3.

IV. DISCUSSION AND CONCLUSION

In this paper, we have achieved NR using a new approach: photonic band gap with surface grating. This approach to NR gives new window for AANR in 2D PCs. This approach also gives flat lens made of these PCs with a large object-image distance. Thus these flat lenses are able to image large and far away objects.

Our new approach gives much larger window of AANR than previous realized. For example for a square lattice air holes in $\epsilon = 12$ with $r/a = 0.35$ studied in Ref. [7], our approach gives a lower limit $\omega_l = 0.183 \times 2\pi c/a$ and an upper limit $\omega_u = 0.206 \times 2\pi c/a$, hence a fraction of AANR frequency range of 11% around $0.206 \times 2\pi c/a$. This range is much larger than the AANR range along the ΓM direction for the TE modes. This window of AANR is easier to locate. The two limits are obtained from the crossing of the band with the light lines around X point and M point, respectively. For the determination of the lower limit ω_l , there is no need to compute the frequency at which the radius of curvature of the contours along ΓM diverges [7].

Our new approach to AANR can also be extended to three-dimensional photonic crystals.

Acknowledgments

This work was supported by the Air Force Research Laboratories, Hanscom through FA8718-06-C-0045 and the National Science Foundation through PHY-0457002.

[1] V. Veselago, Soviet Physics USPEKHI **10**, 509 (1968).

[2] R. A. Shelby, D. R. Smith, and S. Schultz, Science **292**, 77 (2001).

[3] C. G. Parazzoli et al, Phys. Rev. Lett. **90**, 107401 (2003).

[4] V. M. Shalaev, Nat. Photonics **1**, 41 (2007).

[5] J. D. Joannopoulos, R. D. Meade, and J. N. Winn, *Photonic Crystals: Molding the Flow of Light*, Princeton Univ. Press (1995).

[6] M. Notomi, Phys. Rev. B **62**, 10696 (2000).

[7] C. Luo et al, Phys. Rev. B **65**, 201104 (2002).

[8] J. B. Pendry, Phys. Rev. Lett. **85**, 3966 (2000).

[9] P. V. Parimi et al, Phys. Rev. Lett. **92**, 127401 (2004).

[10] P. V. Parimi, W. T. Lu, P. Vodo, and S. Sridhar, Nature (London) **426**, 404 (2003).

[11] E. Cubukcu et al, Nature (London) **423**, 604 (2003).

[12] Z. Lu et al, Phys. Rev. Lett. **95**, 153901 (2005).

[13] P. Vodo, P. V. Parimi, W. T. Lu, and S. Sridhar, Appl. Phys. Lett. **86**, 201108 (2005).

[14] P. Vodo, W. T. Lu, Y. Huang, and S. Sridhar, Appl. Phys. Lett. **89**, 084104 (2006).

[15] D. R. Smith, J. B. Pendry, and M. C. K. Wiltshire, Science **305**, 788 (2004).

[16] A. Berrier et al, Phys. Rev. Lett. **93**, 073902 (2004).

[17] W. T. Lu et al, preprint cond-mat/0702286 (2007).

[18] W. T. Lu and S. Sridhar, Opt. Exp. **13**, 10673 (2005).

[19] Y. Fink et al, Science **282**, 1679 (1998).

[20] A. Taflove and S. C. Hagness, *Computational Electrodynamics: The Finite-Difference Time-Domain Method*, 3rd ed., Artech House Publishers (2005).

[21] X. Zhang, Phys. Rev. B **70**, 205102 (2004); Phys. Rev. E **71**, 037601 (2005).

[22] R. Gajic et al, Phys. Rev. B **73**, 165310 (2006).

[23] Z.-Y. Li and L.-L. Lin, Phys. Rev. B **68** 245110 (2003).